Supplementary Material

Characterization of ofloxacin-imprinted UiO-66-NH_2@RAMIP@BSA

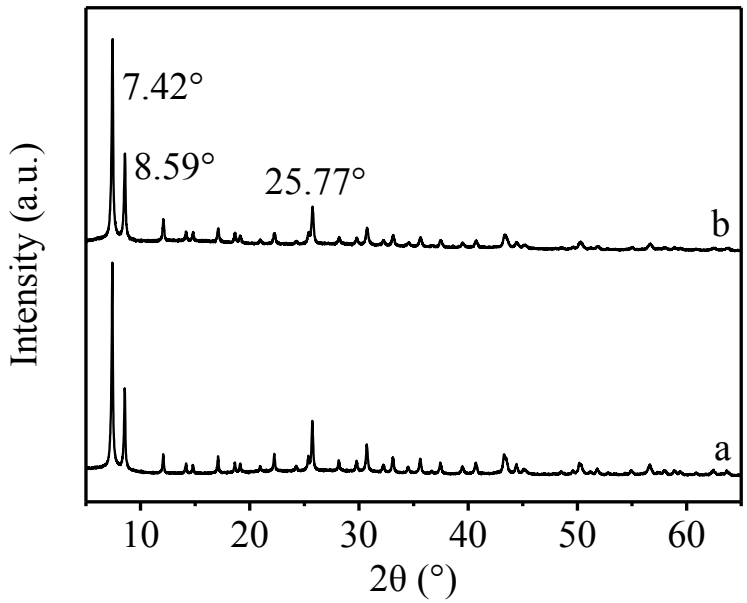

Fig. S1 XRD patterns of (a) UiO-66-NH_2 and (b) UiO-66-NH_2@RAMIP@BSA.

The chemical stability of UiO-66-NH_2 and UiO-66-NH_2@RAMIP@BSA can be seen from the results of x-ray diffractomer patterns (XRD). As shown in Fig. S1, the three main diffraction peaks of UiO-66-NH_2 (2θ =7.42°, 8.59° and 25.77°) coincided with previous report.[16] Compared with XRD of UiO-66-NH_2, three peaks was rarely changed for UiO-66-NH_2@RAMIP@BSA. These results suggested that the crystal structure of UiO-66-NH_2 was not affected by the preparation process. The core had high enough stability to meet the needs of practical applications.

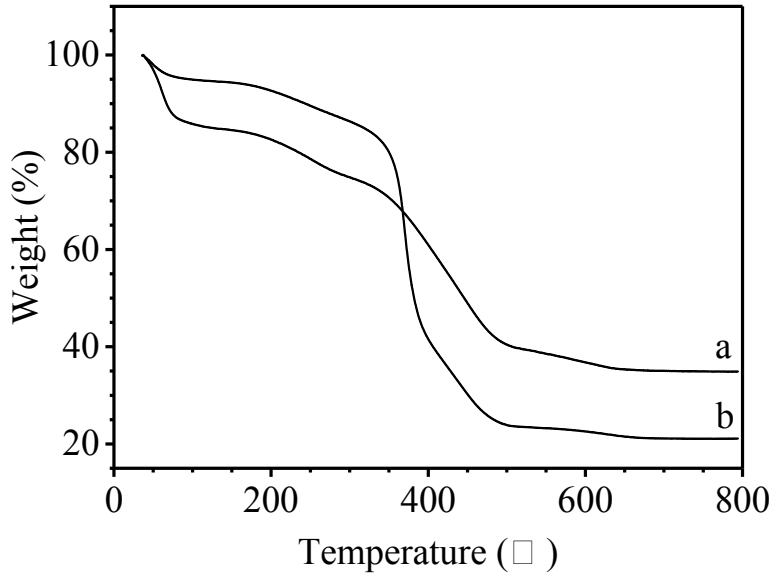

Fig. S2 Thermogravimetric curves of (a) UiO-66-NH_2 and (b) UiO-66-NH_2@RAMIP@BSA.

Fig. S2 showed thermogravimetric curves of UiO-66-NH_2 and UiO-66-NH_2@RAMIP@BSA. Two curves were almost same, and the weight loss was divided into three parts. For UiO-66-NH_2, the loss of weight at about 70 ℃ was due to the evaporation of water molecules. The loss of weight at about 270 ℃ was probably due to the volatilization of DMF which was not replaced by chloroform in the pores. The loss of weight above 350 ℃ was related to the decomposition of UiO-66-NH_2. For UiO-66-NH_2@RAMIP@BSA, the decomposition temperature was reduced to about 200 ℃, which was due to the decomposition of bonded RAMIP layer and BSA, indicating that RAMIP and BSA successfully bonded onto core surface. In the end, the residual ash of UiO-66-NH_2 was more than that of UiO-66-NH_2@RAMIP@BSA, further demonstrating the existence of BSA and RAMIP layer. The thermal stability of UiO-66-NH_2@RAMIP@BSA was good enough for practical application.

Table S1 Adsorption isotherm constants for Langmuir, Freundlich and Langmuir-Freundlich equations

Materials	Langmuir			Freundlich			Langmuir-Freundlich			
	Q_m (mg/g)	K_L (L/mg)	R^2	n	K_F (g/L)	R^2	Q_m (mg/g)	K_L	m	R^2
UiO-66-NH_2@RAMIP@BSA	116.4	0.001142	0.9107	1.235	0.2783	0.9830	88.0	0.0010	1.316	0.9934
UiO-66-NH_2@RANIP@BSA	45.37	0.0005770	0.9355	11.92	0.05329	0.9873	43.5	0.00056	1.069	0.9984

Table S2 The results of kinetics analysis of UiO-66-NH_2@RAMIP@BSA and UiO-66-NH_2@RANIP@BSA

Model	Materials	Equations	$Q_{e,cal}$ (mg/g)	K	R^2
Pseudo first order kinetic model	UiO-66-NH_2@RAMIP@BSA	y=-0.4014x+4.708	110.8	0.4014	0.7540
	UiO-66-NH_2@RANIP@BSA	y=-0.3366x+3.360	28.80	0.3366	0.8502
Pseudo second order kinetic model	UiO-66-NH_2@RAMIP@BSA	y=0.002340x+0.1609	427.4	0.00003400	0.9230
	UiO-66-NH_2@RANIP@BSA	y=0.009100x+0.4927	109.9	0.0001680	0.9913

Table S3 Comparisons between this work and the existing literature in the analysis performance of OFL

NO.	Core materials of MIPs in literature	Q_{max} (mg/g)	Adsorption rate (min)	Recovery (%)	RSD (%)	LODs (ng/mL)	Linearities (ug/L)	References
1	magnetic carboxylated cellulose nanocrystals	45.64	20	81.2-93.7	0.6-7.5	5.4-12.0	-	19
2	Fe_3O_4@SiO_2 nanoparticles	32.7	60	83.1-103.1	0.8-8.2	10.5	100-100000	20
3	poly(glycidyl methacrylate-co-ethylenedimethacrylate) microspheres	5.3	-	82.9-97.5	<9.6	-	1-50	21
4	nanomagnetic polyhedral oligomeric silsesquioxanes	2.255	-	75.6-108.9	2.91-8.87	1.76	50-1000	22
5	polysulfone materials on nickel foam	1.882	30	79.31-107.1	1.7-10.3	1.9	6.2-10000	23
6	Fe_3O_4@SiO_2 nanoparticles	1.455	30	79.2-84.4	2.9-6	18	250-5000	24
7	stainless steel fiber	0.425	20	89.7-103.4	5.8-7.2	-	-	25
8	polymerization methacryclic acid and ethylene glycol dimethacrylate	0.100	-	87.2-97	2.9-4.5	30	70-60000	26
9	inorganic-organic co-functional monomer	0.100	-	87.2-102.9	<5.4	-	200-20000	27
10	spherical silica gel (2 μm)	80.67	25	>83.1, average 95.6	2.47-3.38	0.2	-	28
11	UiO-66-NH_2	50.55	9	93.7-104.2	2.0-4.5	15.6	100-100000	This work